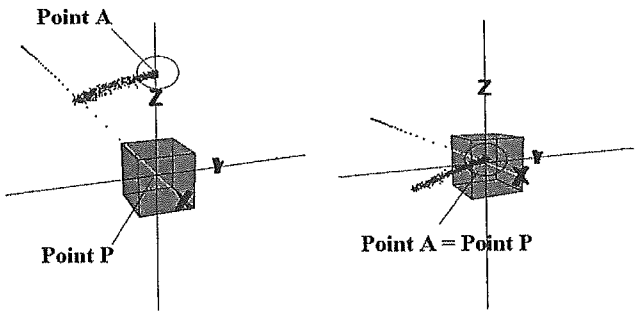

Fig. 1. Trajectory of a marker near a lung tumor in a patient with lung cancer before and after four-dimensional setup. Each spot corresponds to the position of the marker as detected by the real-time tumor-tracking radiotherapy system. In this case, Point P and the gating window (box) were set at the isocenter with 2 mm isotropical "permitted dislocation" from Point P. The actual position of the marker at the end of expiration, Point A, in the trajectory of the marker is adjusted to Point P by moving the treatment couch. The *x*, *y*, and *z* are consistent with the right-left, craniocaudal, and anteroposterior directions, respectively.

tween markers are measured to rule out the possibility of the migration of the markers. The 3D coordinates of the marker that is closest to the tumor are automatically detected 30 times per second by using a real-time pattern-recognition algorithm in which image processors compare the digitized image and the template image of a metallic marker to detect the location of the marker (6). The coordinates of the center of the gold marker were determined using a 16 × 16 pixel image template of the marker. The accuracy of the measurement was estimated to be 0.5 ± 0.2 mm in phantom experiments (4).

In our protocol for lung cancer using the 4D setup, the following steps are involved.

1. After the insertion of the fiducial markers, a multidetector CT is taken as the patient holds his or her breath at the end of expiration, where a previous study of ours found that gating efficiency is highest (7). Transaxial reconstructed CT with a slice thickness of 1 mm is used for treatment planning. Three-dimensional conformal radiotherapy is planned on a 3D radiation treatment planning system. The fiducial marker is contoured on the 3D radiation treatment planning system, and its coordinates relative to the isocenter are transferred to the 4D setup system in the RTRT system. The planned coordinates of the fiducial marker relative to the isocenter are visually demonstrated in a room's-eye view on a display of the 4D setup system as Point P in Fig. 1. The *x*, *y*, and *z* axes correspond to the right-left (RL), craniocaudal (CC), and anteroposterior (AP) directions, respectively. The size of the gating window around Point P can be determined anisotropically in the RL, CC, and AP directions and visualized as a box in the room's-eye view on the display (Fig. 1). In our protocol for lung tumors, the gating window is selected to be isotropic ±2.0 mm for the RL, CC, and AP directions.
2. The RTRT system records the coordinates of the internal fiducial marker for 1 to 2 min at the rate of 30 times per second before the start of treatment. The recorded 3D coordinates of the internal marker are visually demonstrated as the trajectory of the marker in the room's-eye view on a display of the 4D setup system (Fig. 1). Each spot in Fig. 1 corresponds to the coordinates of the marker as detected by the RTRT system 30 times per second.
3. The operator can determine which part of the trajectory is to be used for gating, as follows. One can select the actual coordinates of the marker in the trajectory (Point A). This point can be selected so as to maximize the gating efficiency according to computer guidance. The selected Point A is usually near the end of the expiration phase or near the maximum CC coordinates (the most cranial position) in the trajectory. If the selected point is not near the end of the expiration phase, one can change the position of Point A to be compatible with the point at the end of the expiration phase that was used in the CT planning.
4. In daily radiotherapy, patients are first positioned on the treatment couch with the use of skin markers and lasers in the treatment room.
5. For 1 to 2 min, the coordinates of the fiducial marker, or 3D trajectory, are recorded using the 4D setup system before daily irradiation. This trajectory usually has some interfractional deviation, so the operator needs to determine every day which part of the trajectory, or Point A, would be compatible with the trajectory in the 4D setup system recorded in Steps 1 to 4, according to computer guidance.
6. The table position is shifted by adjusting Point A in the trajectory to the planned position of the marker, Point P, which has been determined in 3D conformal radiotherapy.
7. Real-time tumor-tracking radiotherapy is started using the gating window around Point P. A therapeutic beam is delivered only when the actual position of the marker is within the gating window or within the permitted distance from Point P, as we have reported (1, 4, 6). The linac is enabled during the period that the fiducial marker is within the gating window and

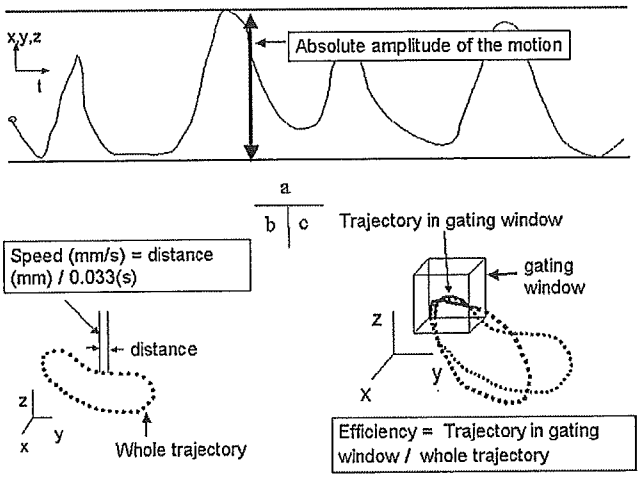

Fig. 2. (a) Absolute amplitude determined from the time signal of the tumor motion in *x*, *y*, and *z* directions. The absolute amplitudes of marker movement were defined as the distance between the maximum and minimum coordinates along each of the axes (*x*, *y*, and *z*) in each log file. (b) Speed of the marker determined from the trajectory of the marker. (c) Efficiency of irradiation determined from the trajectory of the marker and the gating window. We estimated the maximum possible efficiency achieved for each patient with a ±2 mm gating window for the right-left, craniocaudal, and anteroposterior directions.

unenabled when the marker is out of the gating window with the delay of 0.05 s.

Amplitude and speed of the tumor motion

The following study was performed using the data gathered in 21 patients in the 4D setup. The patients were treated with 1 to 8 fractions each for their peripheral lung tumors. The patients were examined with the 4D setup using the RTRT system for 5 days in 2 patients, 4 days in 7 patients, 3 days in 2, 2 days in 6, and 1 day in 4. In total, 60 treatment days, or 3 treatment days on average for each patient, were used for the analysis. The reason why 4D setup was not performed in some treatments was that the researcher was absent on that day; there was no intentional withdrawal of data.

The length of the log file for each 4D setup ranged from 60.8 to 412.1 s, with a mean of 136.4 s. The absolute amplitudes of marker movement were defined as the distance between the maximum and minimum coordinates along each of the axes (x, y, and z) in each log file (Fig. 2a). This definition of absolute amplitude is different from the definition of amplitude in our previous paper, where amplitude was determined as the parameter in a fitting curve assuming sinusoidal respiratory motion (7, 8). Variations in amplitude among patients and also among treatment days for the same patient were examined. The speed of the marker in a 3D trajectory can be determined by dividing the distance between two points by the fluoroscopic imaging pulse sequence of 1/30 s (Fig. 2b). The maximum, minimum, and median speeds of the marker in each log file were examined for each of 60 treatment days in 21 patients. Because RTRT is one type of gating irradiation, it is crucial to estimate the efficiency of therapeutic beam delivery during each treatment session. The 4D setup system can estimate the efficiency of gated irradiation at Point P at a predetermined gating window (Fig. 2c).

In this study, we estimated the maximum possible efficiency achieved for a patient with a ±2 mm gating window for the RL, CC, and AP directions. The actual treatment time using the ±2 mm gating window was recorded in 18 of the 21 patients and compared with the prediction in the 4D setup. The number of readjustments on the treatment couch needed per treatment was recorded in 6 recent patients to figure out the practical effect of baseline shifting and the importance of fine on-line remote control of the treatment couch.

RESULTS

The absolute amplitudes of the trajectories in the x, y, and z directions in 21 patients are shown in Table 1. When the 4D setup data for multiple treatments were available, the absolute amplitude was averaged. In 60 absolute amplitudes along the RL, CC, and AP directions in 21 patients, the number of average absolute amplitudes longer than 10 mm—at which length we found, in a previous study, that gating allowed a meaningful reduction in safety margins (9)—was 20 (33%) (Table 1). The standard deviation of the absolute amplitude was larger than 5 mm in 14 (23%) of 60 (Table 1).

The absolute amplitudes of the trajectories in the x, y, and z directions for 60 treatments in the 21 patients are shown in Fig. 3. When the 4D setup was used several times in the same patient, multiple spots were plotted vertically for that same patient in Fig. 3. Figure 3 shows that the absolute

Table 1. Absolute amplitude and speed of the internal fiducial marker detected in 4D setup system. Average and standard deviation are shown for patients for whom 4D setup was used at least twice. The average at "Total" was calculated as (the sum of the average of each patient)/(number of patients). The standard deviation at Total was for the average of each patient.

Patient no.	4D setup used during irradiation	Average absolute amplitude (mm)			Average speed (mm/s)		
		Right-left	Craniocaudal	Anteroposterior	Max.	Median	Min.
1	4	4.7 ± 1.2	4.7 ± 2.0	5.3 ± 2.6	11.3 ± 3.7	8.2 ± 1.1	6.6 ± 0.7
2	5	4.8 ± 0.5	4.2 ± 0.9	5.5 ± 0.8	43.6 ± 3.6	23.7 ± 0.8	16.2 ± 0.6
3	4	8.0 ± 7.2	17.3 ± 11.0	7.1 ± 2.2	24.7 ± 8.2	10.8 ± 0.4	6.2 ± 0.4
4	1	2.6	3	4.4	11.6	7.6	5
5	2	8 ± 1.6	8.4 ± 2.3	11.7 ± 0.3	36 ± 0.4	10.8 ± 2.0	10.3 ± 1.0
6	2	6.9 ± 6.1	15.1 ± 13.8	11.2 ± 0.0	28.8 ± 0.2	14.3 ± 3.2	9.3 ± 1.2
7	2	2.9 ± 1.6	4.2 ± 2.3	4.4 ± 1.7	8.3 ± 2.3	5 ± 0.2	3.9 ± 0.5
8	1	9.5	13.1	13.7	36.1	26.8	9.1
9	2	2.2 ± 4.3	10.7 ± 1.7	5.2 ± 5.2	8.5 ± 0.3	5.9 ± 0.4	4.6 ± 0.6
10	4	6.2 ± 2.5	17.8 ± 10.1	6.2 ± 2.9	11.5 ± 3.9	7.1 ± 1.4	4.8 ± 0.7
11	4	3.4 ± 0.3	3.6 ± 0.6	3.8 ± 0.3	10.2 ± 0.8	7.4 ± 0.4	6 ± 0.4
12	1	6.4	8.6	5.8	27.6	23.3	18.7
13	4	17.6 ± 9.9	28 ± 3.2	28.4 ± 6.4	54.3 ± 31.9	9.7 ± 0.4	4 ± 1.2
14	2	10.4 ± 10.1	9.9 ± 8.5	8 ± 0.4	23.6 ± 0.3	12.5 ± 0.6	6 ± 0.3
15	5	3.9 ± 1.4	5.7 ± 1.3	3.2 ± 0.7	6.6 ± 0.6	5.5 ± 0.4	4.3 ± 0.6
16	1	6	3.6	2.9	10	7.6	6.1
17	4	19.1 ± 3.7	15.9 ± 7.7	16 ± 5.5	43.6 ± 11.4	23.7 ± 0.4	16.2 ± 2.8
18	2	24.6 ± 7.5	18.3 ± 7.2	19 ± 6.6	72.6 ± 22.5	13.5 ± 8.9	7.2 ± 6.2
19	3	8.3 ± 2.6	21.4 ± 4.3	11.5 ± 3.1	11.3 ± 3.5	6.9 ± 0.5	5.1 ± 0.8
20	3	7.4 ± 0.8	2.1 ± 0.2	2.4 ± 0.8	8.3 ± 0.2	6.6 ± 0.3	5.4 ± 0.5
21	4	8 ± 1.1	8.4 ± 0.6	11.7 ± 1.5	12.6 ± 3.4	7.4 ± 3.6	4 ± 2.2
Total	60	8.2 ± 6.5	10.7 ± 8.6	8.8 ± 7.0	21.1 ± 18.9	9.9 ± 5.4	6.6 ± 3.6

Abbreviation: 4D = four-dimensional.

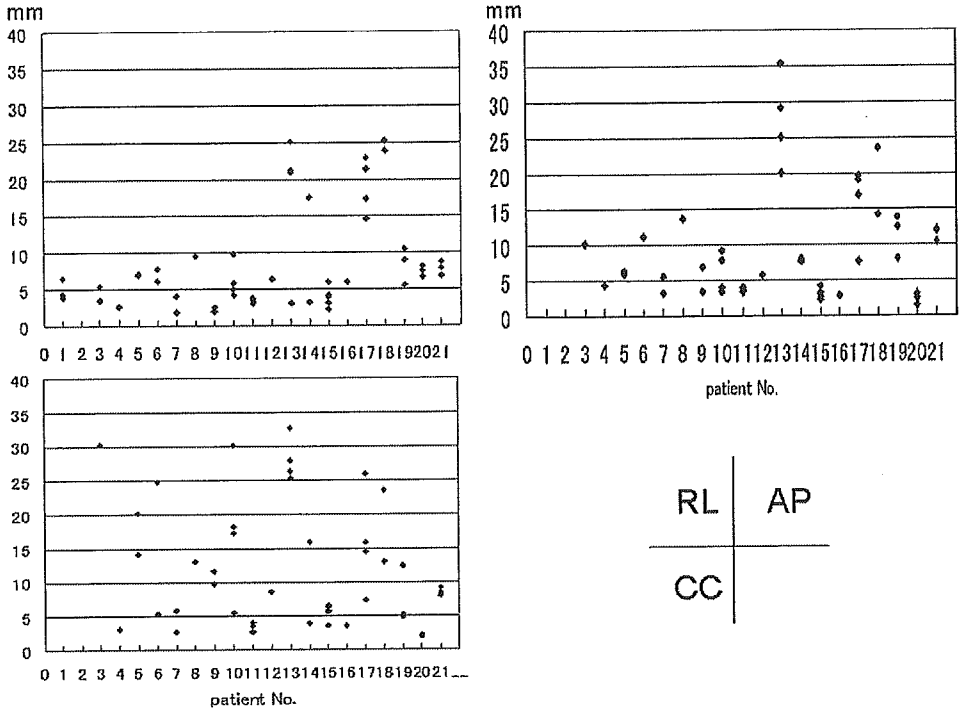

Fig. 3. The absolute amplitudes of the trajectories in right-left, craniocaudal, and anteroposterior directions for 60 treatment days in 21 patients. When the four-dimensional setup was used several times in the same patient, multiple spots were plotted vertically for that same patient. AP = anteroposterior; CC = craniocaudal; R-L = right-left.

amplitude of the marker varied considerably from patient to patient and among treatment days for the same patient. In RTRT, this variation of the absolute amplitude does not worsen the accuracy of the treatment, because the therapeutic beam is delivered only when the marker is within the gating window. However, the larger the absolute amplitude, the longer treatment time tends to be, because the size of the gating window is the same every day.

Some degree of interfractional change in the 3D trajectory of the marker was seen in all patients (Fig. 4). Figure 4 shows typical interfractional and intrafractional changes in marker trajectory from Day 1 to Day 2 in the same patient with lung cancer. It was apparent that the fluctuation of the trajectory was not simple and changed in 3D.

Figure 5 shows the 3D coordinates of the marker at the end of the exhalation and inhalation phases in one patient. The phase in a respiratory cycle was determined by assuming that the maximum and minimum y coordinates in that cycle are consistent with the end of the exhalation and inhalation phases, respectively. Intrafractional change in the coordinates at the end of the inhalation phase was apparent. In this patient, the marker positions at the end of the exhalation phase had a smaller intrafractional variation than those at the end of the inhalation phase.

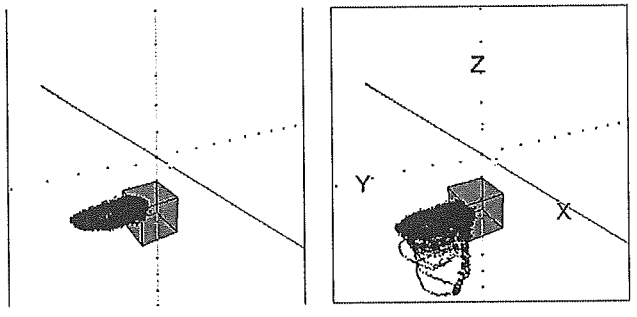

Fig. 4. Interfractional change between Days 1 and 2 in the three-dimensional trajectory of the marker in a patient with lung cancer. The gray box is the gating window. The dots are consistent with the actual positions of the internal fiducial marker detected 30 times per second.

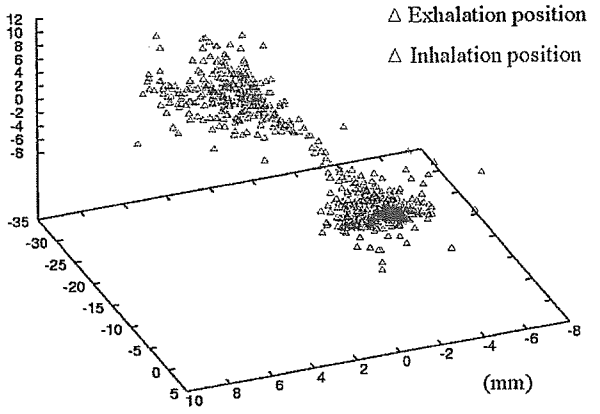

Fig. 5. Three-dimensional coordinates of the marker at the end of exhale phase (blue) and inhale phase (red) in 1 patient.

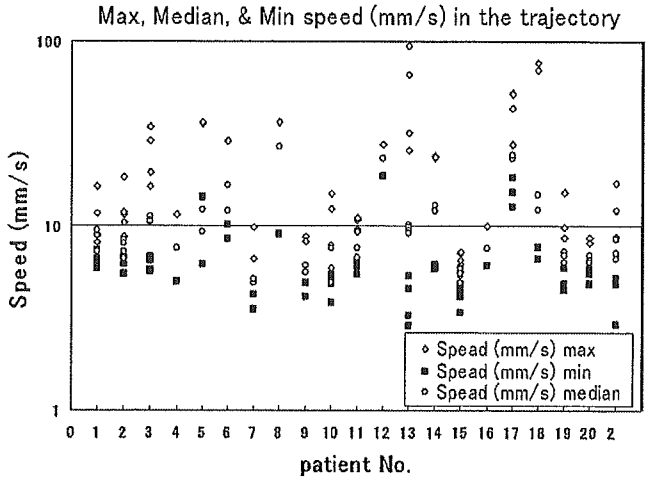

Fig. 6. The maximum, minimum, and median speeds of the marker for 60 treatment days in 21 patients are plotted in log scale.

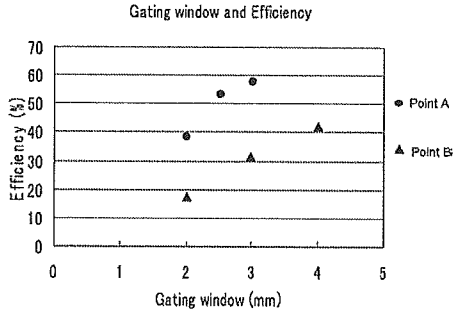

Fig. 8. The relationship between the size of the gating window and the maximum efficiency achievable in 1 patient. Point A is the maximum efficiency achievable as predicted by the four-dimensional setup system and examined at the gating window of ±2.0, ±2.5, and ±3 mm. Point B is a point arbitrarily determined by an operator without the help of the system at the gating window of ±2.0, ±3.0, and ±4.0 mm.

Figure 6 shows the maximum, median, and minimum speeds of the marker (log scale) for 60 treatment days in 21 patients. It was apparent that the median speed is closer to the minimum than to the maximum speed in the majority of patients, but the median speed is close to the maximum on a few occasions. In 10 (16%) of the 60 treatments, the maximum marker speed exceeded 33 mm/s, which has been reported to be the average maximum leaf velocity at the isocenter plane of the multileaf collimator by Wijesooriya *et al.* (10). The highest average maximum speed in the present study was 94 mm/s, whereas the average maximum speed of the marker was more than 33 mm/s in 6 (29%) of 21 patients (Table 1).

Figure 7 shows the maximum efficiency of the irradiation achievable with the ±2 mm gating window for the RL, CC, and AP directions. The achievable efficiency varied considerably among patients. Even in the same patient, the achievable efficiency of the irradiation varied considerably among treatment days. Figure 8 shows how the maximum achievable efficiency changed with the size of the gating window from ±2.0, 2.5, and 3.0 mm for Point A, which is determined using 4D setup, and ±2.0, ±3.0, and ±4.0 mm for Point B, which is arbitrarily determined, respectively. Higher gating efficiency was predicted when we determined the Point A for gating using the 4D setup system rather than when we selected an arbitrary Point B without the help of this system. The larger gating window would be needed for Point B to achieve similar efficiency, so that normal tissue would be irradiated more when we use Point B for gating rather than Point A.

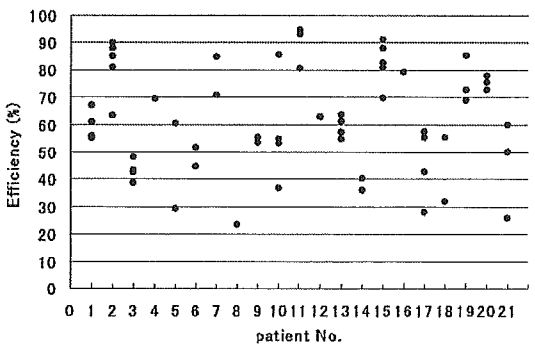

Fig. 7. The maximum efficiency of the irradiation achievable with the ±2 mm gating window for *x*, *y*, and *z* directions for 60 treatment days in 21 patients.

Table 2 shows the number of readjustments of the table position needed as a result of the baseline shift of the marker trajectory during RTRT in 6 patients. The achievable efficiency of the gated radiotherapy was 62.4% ± 19.0% predicted by the calculation of the 4D setup system if we used ±2 mm for the gating window. The actual treatment time was 25 ± 13 min for 10.5 ± 1.7 Gy. The actual efficiency was grossly estimated as 28% (10.5 Gy in 7 min vs. 10.5 Gy in 25 min), assuming a dose rate of 1.5 Gy/min, the most frequent rate of the linear accelerator in gating mode. The number of readjustments needed during irradiation as a result of a baseline shift of the tumor position in most patients was 4.1 ± 4.1 times per treatment day. One patient needed 21 readjustments on his initial treatment day, because he had difficulty resting quietly on the treatment couch.

DISCUSSION

Engelsman *et al.* assessed the impact of both setup errors and respiration motion on the cumulative dose delivered to a clinical target volume in the lung and found that systematic setup errors have a dominant effect on the cumulative dose to the clinical target volume; random setup errors and breathing motion have smaller effects (9). Accordingly, they recommended minimizing systematic setup errors for lung tumors in motion. Bony landmarks have been used as surrogates for the setup of the lung tumor by comparing megavoltage portal images with simulation film or digitally reconstructed radiographs (11). Reports using CT simula-

Table 2. Number of treatments, daily dose, achievable efficiency estimated by the four-dimensional setup system, actual total treatment time, and readjustments of the treatment couch per treatment. The mean total treatment time was calculated as (total treatment time)/(number of patients examined). The standard deviation in the "Total" row was for the mean time of each treatment. The number in the column "Readjustments per treatment" is the number of readjustments per treatment day including the initial setup. Each number corresponds to the number of required readjustments on the 1st, 2nd, 3rd, and 4th treatment days from left to right.

Patient no.	Number of treatments	Daily dose (Gy)	Achievable efficiency (%)	Total treatment time (minutes)	Readjustments per treatment (including one setup time)
1	4	10	59.7	35 ± 27	–*
2	8	6	81.4	—	–*
3	4	12	43.1	36 ± 8	–*
4	4	10	69.4	10 ± 1	–*
5	4	12	44.9	34 ± 13	–*
6	4	12	48.1	23 ± 4	–*
7	4	10	77.8	12 ± 1	–*
8	4	10	23.5	17 ± 3	–*
9	4	10	44.1	14 ± 1	–*
10	4	10	57.6	19 ± 3	–*
11	4	10	90.4	9 ± 1	–*
12	1	15	62.9	—	–*
13	4	10	59.2	—	–*
14	4	10	38.3	28 ± 7	–*
15	4	12	82.4	17 ± 0	–*
16	4	10	79.1	15 ± 4	2, 3, 3, 2
17	4	10	45.9	28 ± 3	21, 6, 3, 2
18	4	10	43.7	31 ± 5	4, 5, 3, 2
19	4	12	75.7	17 ± 2	2, 2, 5, 2
20	4	10	75.3	21 ± 4	2, 3, 3, 2
21	4	10	48.9	41 ± 18	5, 5, 2, 10
Total	85	10.5 ± 1.7	62.4 ± 19.0	25 ± 13	4.1 ± 4.1

* No data available.

tion did, however, raise questions about the reliability of bony landmarks for the positioning of lung tumors (12, 13).

The present findings showed that the variation of the absolute amplitude of the trajectory among patients was remarkable not only in the craniocaudal direction but also in the lateral and anterodorsal directions. Four-dimensional planning using CT images at different respiratory phases, or usage of 4DCT, has been useful for determining the different internal target volumes for individual patients, incorporating changes in the position and shape of the tumor (14–17). These techniques are useful for assessing the magnitude of respiratory motion, to the extent that the motion is reproducible or negligible. However, we have found that the magnitudes of the interfractional and intrafractional changes in the same patient were often remarkable in terms of absolute amplitude. The variation was large not only in the CC direction but also in the RL and AP directions. Our study suggests that, in planning with 4DCT, it is important to estimate the residual uncertainty of tumor motion with respect to its interfractional and intrafractional changes.

To reduce interfractional and intrafractional errors due to variation in the motion of the tumor, real-time tracking technology is now expected to be useful and practical. In the use of real-time tracking technology in radiotherapy, two concepts have been reported. One is *intercepting radiotherapy,* in which a therapeutic beam is gated to irradiate a tumor at a planned position by intercepting the trajectory of the tumor motion. This has been used for lung tumors with the RTRT system developed at our institution. The shortcoming of the intercepting radiotherapy is lower efficiency than conventional nongated radiotherapy. The present study showed that even with a table shift, the achievable gating efficiency is only 62.4% ± 19%, which has room for improvement. The other method reported is *pursuing radiotherapy,* in which the position of the tumor is monitored using real-time tracking technology, and the moving aperture of a linear accelerator is synchronized with the tumor's motion to irradiate the tumor continuously (5, 18, 19). The latter method is expected to increase efficiency and decrease treatment time. Precise prediction of tumor motion is expected to be useful to decrease treatment time (20). Previous data have been predicted well with some mathematical models (21, 22). However, the present study showed that the speed of the tumor varied considerably during a single treatment session and among treatment days in the same patient. Some patients' tumors move as fast as 90 mm/s, so mechanical control of the aperture for pursing radiotherapy may be difficult without some cutoff level for the speed to follow, as Wijesooriya *et al.* reported (10). Interestingly enough, the present study showed that the variation in median and minimum speeds was not as large as that in median and maximum speeds (Table 2). This finding is

consistent with the steadiness of the 3D tumor position at the expiratory phase shown in Fig. 5 and in our previous analysis (7). The relative steadiness of the speed and the position at the expiratory phase shown in this study will be important in the design of 4DRT in future. Meanwhile, intercepting radiotherapy rather than pursuing radiotherapy is safer and most cost-effective in clinical use.

Frequent correction of the treatment couch during the delivery of irradiation was as important as the setup at the start of irradiation. Any emotional change of the patient, as well as any unintentional sigh, cough, or abdominal distention, can induce a change in the tumor trajectory (8). The need for frequent and prompt correction strongly suggests the importance of fine on-line remote control of the treatment couch from outside the treatment room in intercepting radiotherapy. Otherwise, radiotherapists would be required to go into the treatment room too many times to adjust the treatment couch during the delivery of radiotherapy. The 4D setup system was useful for increasing the efficiency of gated irradiation by selecting the best position for gating. The actual efficiency of 28% in the 21 patients in our study was not detrimental, although it was less than the best achievable efficiency, 62.4%, predicted by the 4D setup. The reason why actual efficiency was lower than the predicted one may be explained by the learning curve necessary to use the 4D setup system efficiently. Otherwise, it may be due to the difference in the trajectory between the prediction and the actual treatment, because of the large intrafractional change of the trajectory. If the latter is the main reason, the 4D setup system is to be modified for increasing efficiency. However, we are not yet certain which explanation is correct, because only a few researchers have had the opportunity to use the 4D setup system so far.

Four-dimensional setup using the tumor trajectory in the RTRT system can minimize the systematic setup error between the tumor position at the planning CT and the tumor position at the actual treatment at the same respiratory phase, as long as the fiducial marker is stable. Even if there is a large interfractional change in the tumor position relative to bony landmarks, the risk of geographically missing the target volume will be reduced with the 4D setup. The main limitations of this setup are as follows: (*1*) possible migration of the fiducial marker from the implanted position, (*2*) possible deformation of the tumor during radiotherapy, and (*3*) lack of awareness about the relationship between the marker and the critical organ. The first two limitations could be reduced by using 3 fiducial markers around the tumor or by adding CT-on-rail in the treatment room. We reported earlier that the reliability of the marker position lasts for 2–4 weeks from the start of radiotherapy, beyond which the deformation of the lung due to inflammation and tumor shrinkage makes the position unreliable (23). Now at our institution, 3 or 4 markers are implanted around the tumor and used to detect the possible migration before treatment (23).

In conclusion, substantial interfractional and intrafractional changes in the absolute amplitude and speed of lung tumors were detected. Because the determination of internal target volume using 4DCT, prediction models of respiratory motion, and pursuing RT systems are all vulnerable to these changes in the absolute amplitude and speed of lung tumors, more work is required to polish 4DRT. The 4D setup using the trajectory of tumor motion with fine on-line remote control of the treatment couch was shown to be useful for reducing the uncertainty of tumor motion and for increasing the efficiency of gated irradiation.

REFERENCES

1. Shirato H, Shimizu S, Kitamura K, *et al.* Four-dimensional treatment planning and fluoroscopic real-time tumor tracking radiotherapy for moving tumor. *Int J Radiat Oncol Biol Phys* 2000;48:435–442.
2. Keall PJ, Starkschall G, Shukla H, *et al.* Acquiring 4D thoracic CT scans using a multislice helical method. *Phys Med Biol* 2004;49:2053–2067.
3. Underberg RW, Lagerwaard FJ, Cuijpers JP, *et al.* Four-dimensional CT scans for treatment planning in stereotactic radiotherapy for stage I lung cancer. *Int J Radiat Oncol Biol Phys* 2004;60:1283–1290.
4. Shirato H, Shimizu S, Kunieda T, *et al.* Physical aspects of a real-time tumor-tracking system for gated radiotherapy. *Int J Radiat Oncol Biol Phys* 2000;48:1187–1195.
5. Neicu T, Shirato H, Seppenwoolde Y, *et al.* Synchronized moving aperture radiation therapy (SMART): Average tumour trajectory for lung patients. *Phys Med Biol* 2003;48: 587–598.
6. Shimizu S, Shirato H, Ogura S, *et al.* Detection of lung tumor movement in real-time tumor-tracking radiotherapy. *Int J Radiat Oncol Biol Phys* 2001;51:304–310.
7. Seppenwoolde Y, Shirato H, Kitamura, K, *et al.* Precise and real-time measurement of 3D tumor motion in lung due to breathing and heartbeat, measured during radiotherapy. *Int J Radiat Oncol Biol Phys* 2002;53:822–834.
8. Shirato H, Seppenwoolde Y, Kitamura K, *et al.* Intrafractional tumor motion: Lung and liver. *Semin Radiat Oncol* 2004;14:10–18.
9. Engelsman M, Damen EM, De Jaeger K, *et al.* The effect of breathing and setup errors on the cumulative dose to a lung tumor. *Radiother Oncol* 2001;60:95–105.
10. Wijesooriya K, Bartee C, Siebers JV, *et al.* Determination of maximum leaf velocity and acceleration of a dynamic multileaf collimator: Implications for 4D radiotherapy. *Med Phys* 2005;32:932–941.
11. Van Sornsen de Koste JR, de Boer HC, Schuchhard-Schipper RH, Senan S, Heijmen BJ. Procedures for high precision setup verification and correction of lung cancer patients using CT-simulation and digitally reconstructed radiographs (DRR). *Int J Radiat Oncol Biol Phys* 2003;55:804–810.
12. Wulf J, Hadinger U, Oppitz U, *et al.* Stereotactic radiotherapy of extracranial targets: CT-simulation and accuracy of treatment in the stereotactic body frame. *Radiother Oncol* 2000; 57:225–236.
13. Fung AY, Grimm SY, Wong JR, *et al.* Computed tomography localization of radiation treatment delivery versus conventional localization with bony landmarks. *J Appl Clin Med Phys* 2003;4:112–119.
14. Shirato H, Shimizu S, Bo X, *et al.* Four-dimensional (4-D) treatment planning integrating respiratory phases and three-dimensional (3-D) movements of lung and liver tumors using

high-speed computed tomography (CT) and magnetic resonance imaging (MRI). In: Lemke MW, Inamura K, Farman A, editors. Computer assisted radiology and surgery. San Diego: Elsevier Science; 1998;265–270.
15. Vedam SS, Keall PJ, Kini VR, *et al.* Acquiring a four-dimensional computed tomography dataset using an external respiratory signal. *Phys Med Biol* 2003;48:45–62.
16. Underberg RW, Lagerwaard FJ, Cuijpers JP, *et al.* Four-dimensional CT scans for treatment planning in stereotactic radiotherapy for stage I lung cancer. *Int J Radiat Oncol Biol Phys* 2004;60:1283–1290.
17. Rietzel E, Chen GT, Choi NC, *et al.* Four-dimensional image-based treatment planning: Target volume segmentation and dose calculation in the presence of respiratory motion. *Int J Radiat Oncol Biol Phys* 2005;61:1535–1550.
18. Murphy MJ. Tracking moving organs in real time. *Semin Radiat Oncol* 2004;14:91–100.
19. Berbeco RI, Jiang SB, Sharp GC, *et al.* Integrated radiotherapy imaging system (IRIS): Design considerations of tumour tracking with linac gantry-mounted diagnostic x-ray systems with flat-panel detectors. *Phys Med Biol* 2004;49:243–255.
20. Vedam SS, Keal PJ, Docef A, *et al.* Predicting respiratory motion for four-dimensional radiotherapy. *Med Phys* 2004;31: 2274–2283.
21. Sharp GC, Jinag SB, Shimizu S, *et al.* Prediction of respiratory tumour motion for real-time image-guided radiotherapy. *Phys Med Biol* 2004;49:425–440.
22. Wu H, Sharp GC, Salzberg B, *et al.* A finite state model for respiratory motion analysis in image guided radiation therapy. *Phys Med Biol* 2004;49:5357–5372.
23. Imura M, Yamazaki K, Shirato H, *et al.* Insertion and fixation of fiducial markers for setup and tracking of lung tumors in radiotherapy. *Int J Radiat Oncol Biol Phys* 2005;63:1442–1447.

Characteristics of Patients Who Developed Radiation Pneumonitis Requiring Steroid Therapy After Stereotactic Irradiation for Lung Tumors

Masaharu Fujino, MD,[a] Hiroki Shirato, MD,[a] Hiroshi Onishi, MD,[e] Hidemasa Kawamura, MD,[b] Kenji Takayama, MD,[d] Masashi Koto, MD,[d] Rikiya Onimaru, MD,[a] Yasushi Nagata, MD,[c] Masahiro Hiraoka, MD[c]

BACKGROUND

To find possible risk factors for symptomatic radiation pneumonitis (RP) after stereotactic irradiation (STI) for peripheral non-small cell lung cancer (NSCLC), pre-treatment pulmonary function test and dose volume statistics in patients who developed RP requiring steroid intake were retrospectively compared with statistics of those who did not develop RP.

MATERIALS AND METHODS

From 1996 to 2002, 156 patients with Stage I NSCLC received STI at 5 hospitals in Japan. Of those patients, 12 were medicated with steroids for RP after treatment (RP group). For comparison, 31 patients were randomly selected from the remaining 144 patients who received STI but did not receive steroids (control group).

RESULTS

There were no statistical differences in age, sex, tumor size, performance status, forced expiratory volume in 1 sec ($FEV_{1.0}$%), or percent vital capacity (%VC) between patients medicated with steroids for RP and those who did not have RP and received no steroids. V_{20} (%) was 7 to 18% (median 8%) in patients medicated with steroids for RP and 2 to 16% (median 7%) in those who did not have RP. No difference was observed in V_{20}, the biologically effectively dose (BED) at the periphery of the planning target volume, or the dose per fraction between the two groups.

CONCLUSIONS

Pre-treatment pulmonary function test (%VC, $FEV_{1.0}$%), and dose volume statistics (V_{20}, total dose, BED, dose per fraction, peripheral dose) were not predictive of RP requiring steroid intake after STI for stage I NSCLC. *(Cancer J 2006;12:41–46)*

KEY WORDS

Stereotactic irradiation, radiation pneumonitis, respiratory function

From the [a]Department of Radiology, Hokkaido University School of Medicine, Hokkaido, Japan; [b]Department of Radiology, Tokyo Metropolitan Komagome Hospital, Tokyo, Japan; [c]Department of Radiology, Kyoto University School of Medicine, Kyoto, Japan; [d]Department of Radiology, Tohoku University School of Medicine, Sendai, Japan; [e]Department of Radiology, Yamanashi Medical College, Tamaho-cho, Japan.

Received on September 14, 2005; accepted for publication October 12, 2005.

No benefits in any form have been or will be received from a commercial party related directly or indirectly to the subject of this article.

This study has been presented at the ASTRO 46th annual meeting in Atlanta, Georgia, October 3–7, 2004.

Reprint requests: Masaharu Fujino, Department of Radiology, Hokkaido University School of Medicine, North-15 West-7, Sapporo, Japan.

E-mail: mfujino@radi.med.hokudai.ac.jp

Three-dimensional conformal radiotherapy has been expected to improve the outcome of stage I non-small cell lung cancer (NSCLC) but has often failed[1] possibly because of the inadequate dose for local control.[2] Stereotactic irradiation (STI), or small-volume high-dose hypofractionated irradiation in a short treatment time, has been shown to be effective with a low risk of symptomatic radiation pneumonitis (RP) for peripheral stage I NSCLC.[3–8]

Recently, nine Japanese institutions have cooperated on retrospectively analysis of treatment outcomes of STI for 245 patients with stage I NSCLC.[8] The general treatment outcome has already been published.[8] In short, during follow-up (median, 24

months; range, 7–78 months), the local recurrence rate was 8.1% for biologically equivalent dose (BED) of 100 Gy or more compared with 26.4% for < 100 Gy using α/β of 10 ($P < 0.05$). The 3-year overall survival rate of medically operable patients was 88.4% for BED of 100 Gy or more compared to 69.4% for BED < 100 Gy ($P < 0.05$). Grade 2, Grade 3 and 4 (National Cancer Institute Clinical Toxicity Criteria, Version 2.0) RP was observed in 4.1%, 1.3%, and 1.3% of cases, respectively. A small proportion of the patients were reported to have received steroids for their symptomatic RP.[3–8] Although the symptoms have been reported to be transient, there is great interest in predicting the onset of symptomatic RP after STI.

In this study, to find possible risk factors for symptomatic RP after STI, the pulmonary function and dose volume statistics in patients who developed RP were retrospectively investigated. Five of the nine institutions mentioned above agreed to participate in this retrospective study to analyze the dose volume statistics as well as other characteristics of the patients.

The risk of RP requiring steroids was known to be related to the percent of volume that was irradiated by 20 Gy relative to the bilateral total lung volume minus planning target volume (V_{20}).[9] Multivariate analysis revealed V_{20} to be the sole independent predictor of RP in Graham et al.'s analysis.[9]

Although other parameters, such as mean lung dose or mean of normalized total dose,[10] could predict the risk of RP better than V_{20}, we selected V_{20} in this study since V_{20} had been routinely measured in these five institutions during the actual treatment. We have used steroid intake for RP treatment as an objective indicator of the severity of RP.

MATERIALS AND METHODS

Stereotactic techniques fulfilled three requirements: 1) reproducibility of the iso-center <5 mm, as confirmed in every fraction; 2) slice thickness on CT scan <3 mm for three-dimensional treatment planning; and 3) irradiation with multiple non-coplanar static ports or dynamic arcs.[8] To fulfill the first requirement, CT images using either CT on rail, two-directional portal graphs, or fluoroscopic verification of a fiducial marker near the tumor, were acquired before every treatment.

Treatment planning with irregularly shaped beams using non-coplanar multiple dynamic arcs or multiple static ports (6–20 ports) was established with the help of a 3D treatment-planning computer. Beam shaping was performed using an integrated motorized multileaf collimator with 0.5- to 1-cm leaf width at the isocenter. Various techniques using breathing control or gating methods and immobilization devices such as a vacuum cushion with or without a stereotactic body frame were utilized to reduce respiratory internal margins. The periphery of the planning target volume received 80%–90% of the prescribed dose.

Planning CT scans were generally performed with 2- or 3-mm slice thickness and displayed using a window level of –700 Hounsfield units (HU) and a window width of 2000 HU. Irradiation and planning CT scans were performed under breath-hold conditions in two institutions and under free shallow breathing with images taken using slow scanning (4 seconds per slice) in three institutions.

The clinical target volume (CTV) marginally exceeded the macroscopic target volume by 0–5 mm. The planning target volume (PTV) comprised the CTV, a 2- to 5-mm internal margin, and a 5-mm setup margin. Using STI, a high dose was concentrated on the tumor-bearing area while the surrounding normal lung tissues were largely spared.

Irradiation schedules also differed among institutions. The number of fractions ranged between 2 and 25, with single doses of 3–12 Gy. A total dose of 18–75 Gy at the isocenter in 2–25 fractions was administered with 6-MV X-rays within 20% heterogeneity in the PTV dose. No chemotherapy regimens were administered before or during radiotherapy.

To compare the effects of various treatment protocols with different fraction sizes and total doses, BED was utilized in a linear-quadratic model.[11] BED was defined as $nd(1+d/(\alpha/\beta))$, with units of Grays, where n is the fractionation number, d is the daily dose, and α/β is assumed to be 2 for normal lung tissue. BED was not corrected with values for tumor doubling time or treatment term.

From 1996 to 2002, in 156 patients receiving STI for peripheral NSCLC at 5 hospitals, 12 (7.6%) were medicated with steroids for post-treatment RP. These 12 patients (8 male, 4 female) are the subjects in this study. Their median age was 72 and ranged from 56 to 86. There were 6 T1N0M0 and 6 T2N0M0 patients. The maximum diameters of the tumors ranged from 12 to 46 mm, with a median of 32 mm. The respiratory function data and dose volume statistics were obtained retrospectively and thus not all the data were corrected for all parameters.

For comparison, the remaining 144 patients who received STI but did not receive steroids can be considered as a control group. However, the present series contains patients treated between 1996 and 2002. Graham et al.'s paper about V_{20} has published in 1999.[9] Many of the patients were treated without taking the V_{20} data at the time of treatment. Thus, we needed to re-load the CT and treatment planning data for this retrospective analysis. Statistical evaluation

persuades us to select 31 patients randomly from the remaining 144 patients who received STI but did not receive steroids as a control group (Table 1). There were 18 T1N0M0 and 13 T2N0M0 patients. The maximum diameters of the tumors ranged from 13 to 58 mm, with a median of 30 mm in the control group.

RESULTS

There were no statistical differences in age, sex, tumor size, and performance status between patients medicated with steroids for RP (RP group) and those who did not have RP and consequently received no steroid treatment (control group) (Table 1).

Pulmonary function tests before STI and dose volume statistics are shown in Table 1. There was no difference in the mean value of $FEV_{1.0}$% before STI between the 6 patients in the RP group and the 26 patients in the control group for whom pre-STI respiratory function data had been collected. Also, there was no difference in the mean value of volume capacity (%VC) between two groups. The number of patients for whom diffusion capacity for carbon monoxide (DLco) had been examined was too small to make a comparison on that basis. Three patients in the RP group had used oxygen intake before STI for poor respiratory function, compared to one patient in the control group. None of these patients required an increase of oxygen supply after STI. One patient in the RP group who did not initially require oxygen began to receive oxygen after STI. Thus, the overall incidence of RP requiring oxygen was 0.6% (1/156).

Distribution of $FEV_{1.0}$% and %VC, which are known to be related to the characteristic of the underlying lung disease, were not different between the 6 patients in the RP group and the 26 patients in the STI group, as shown in Figure 1.

Total physical dose, dose per fraction, BED with the α/β ratio of 2 at the isocenter and at the periphery of the PTV were not different between two groups (Table 2). In the RP group, V_{20} was distributed from 7 to 18% with a median of 8%, while in the control group it was distributed from 2 to 16% with a median of 7%. There was no statistically significant difference in V_{20}. Distribution of BED at the periphery of PTV and V_{20} were not different between the RP and control groups as shown in Figure 2.

DISCUSSION

Graham et al. found by multivariate analysis that V_{20} was the best predictor of RP requiring steroid therapy after three-dimensional radiotherapy.[9] They have shown that RP requiring steroids by 24 months de-

TABLE 1 Characteristics of Patients

Characteristics	RP Group	Control Group	*P* value
Number of patients	12	31	–
Gender			Not significant
Male	8	22	–
Female	4	9	–
Median age in years (range)	72 (56 ~ 86)	49 ~ 87 (76)	0.1364
Median tumor size (mm) (range)	32 (12 ~ 46)	30 (14 ~ 58)	0.4606
Clinical stage			Not significant
IA	6	18	
IB	6	13	
Performance States			0.8555
0	1	10	
1	9	12	
2	0	7	
3	0	2	
Unevaluated	2	0	
Pretreatment %VC			0.3087
N	6	26	
Median (range)	79.1 (45.4–153)	92.6 (60.0–119)	
Pretreatment $FEV_{1.0}$%			0.484
N	6	26	
Median (range)	73.6(56.6–83.9)	64.5(28.1–100)	
Pretreatment DLco (mL/min/mmHg)			0.1649
N	4	9	
Median (range)	10.02 (5.79–13.5)	5.03 (2.50–16.7)	

Abbreviations: %VC, % vital capacity; $FEV_{1.0}$%, forced expiratory volume in 1 sec %; *N*, number of patients measured; DLCo, diffusion capacity for carbon monoxide.

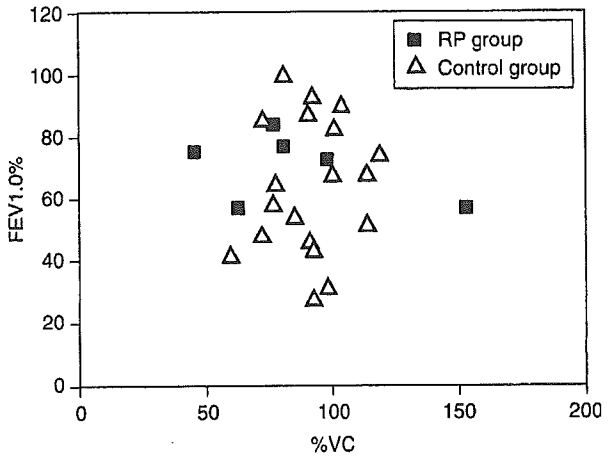

FIGURE 1 Distribution of %VC and $FEV_{1.0}$% for the RP and control groups.

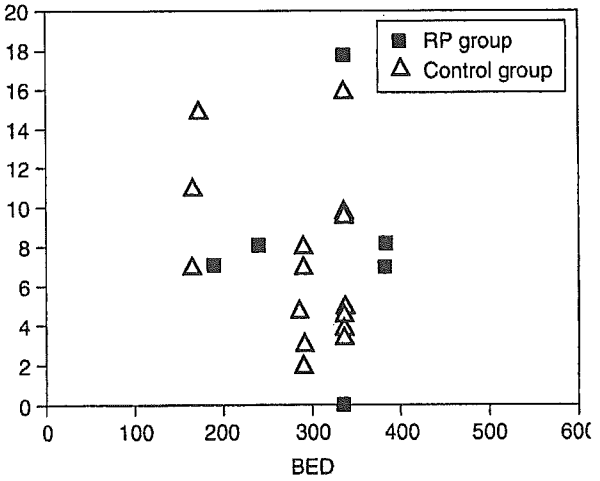

FIGURE 2 Distribution of BED at the periphery of PTV and V_{20} (%) for RP and control groups.

veloped in 0%, 7%, and 13% in patients who had V_{20} at <22%, 22%–31%, and 32%–40%, respectively and grade 3–5 RP (requiring oxygen therapy or more severe) developed in 0%, 8%, 5% (1 fatal), and 23% (3 fatal) of patients who had V_{20} at <22%, 22%–31%, 32%–40%, and > 40%. Other studies have confirmed the relationship between V_{20} and incidence of symptomatic RP.[12,13]

Because none of the patients in the present study had V_{20} more than 22%, there theoretically should have been no patients who required intake of steroids. However, 7.6% of patients in the present series required steroid intake. This contradicts the prediction from Graham et al.'s study.[9] There were only a small number of patients (around 10) who had V_{20} < 22 Gy in Graham et al.'s series, so that there was a large confidence interval at the low dose area of their analysis. This may be the reason for the discrepancy of the prediction. Another possibility is the large fractional doses administered to our subjects. The biologically equivalent dose must have been larger than that of three dimensional conformal radiotherapy (3D-CRT), which is used in conventional fractionation: the volume receiving a lower total dose such as V_{15} or V_{10} might have been more predictive of the incidence of RP after STI. Lee et al have found that addition of chemotherapy to radiotherapy is required when using V_{10} rather than V_{20} to find statistically significant differences in the incidence of RP[14]; however, there were no patients who received chemotherapy in our series. There are other studies which have suggested that the mean lung dose is also a predictor of RP requiring steroids.[10,15,16] Seppenwoolde et al have suggested that the underlying dose-effect relation for RP was linear rather than a step function showing the mean lung dose would be the useful predicting parameter.[10] Prospective analysis is needed to find the answer to this question.

In the literature, it is still debatable whether pulmonary function tests are predictive of RP. Robnett et al. have reported that when analyzed by the median $FEV_{1.0}$ (1.9 liters), patients with pulmonary function below the median had a severe-RP rate of 13%, compared with 6% for patients with an $FEV_{1.0}$ above the median.[17] $FEV_{1.0}$ was not associated with a risk of se-

TABLE 2 Dose Volume Statistics

	RP Group	Control Group	*P* value
Isocenter Dose			
Median physical dose (Gy) (range)	48 (40–75)	60 (40–72.5)	0.7452
Median BED (range) [α/β = 2]	290 (165–382.5)	290 (165–510)	0.0986
Median dose per fraction (Gy) (range)	6 (3–15)	7.5 (3–15)	0.4628
Peripheral dose			
Median physical dose (Gy) (range)	46 (38–71)	48 (32–63)	0.9676
Median BED (range) [α/β = 2]	231 (152–343)	231 (148–463)	0.1014
Median dose per fraction (Gy) (range)	6 (3–15)	7.5 (3–15)	0.3573
N	7	18	
Median V_{20}(%) (range)	8 (7–18)	7 (2–16)	0.15

vere RP in their series ($P < 0.90$). Inoue et al have shown that $PO_2 < 80$ torr and high CRP (>1.0 ng/mL) were associated with a higher rate of RP.[18] However, they have found no relationship between $FEV_{1.0}$% or %VC and RP. Pulmonary symptoms were associated with a DLco loss of >30% ($P = 0.003$) in Gopal et al.[19] The existence of a clinical diagnosis of chronic obstructive pulmonary disease was reported to be a prognostic factor in one study.[16] Patients with lung cancer had a significantly higher risk of RP than patients with lymphoma/breast cancer, which may reflect differences in baseline pulmonary function.[15] However, other studies did not see any relationship between these factors.[9,20,21] Marks et al have suggested the use of multiple factors for prediction.[21] Recently, Lind et al have assessed the utility of dosimetric/functional metrics as predictors of symptomatic RP using receiver operating characteristic curves for 277 patients.[22] They have found that the models using pretreatment pulmonary function, mean lung dose, and perfusion-weighted lung dose were best correlated with outcome (ROC area: 0.7) but were still not sufficient to be recommended as predictors. Many of the patients in this study have not examined pulmonary function testing before the treatment and thus prospective study is required to examine the predictive value of pulmonary function tests before STI.

This study demonstrated that pre-treatment pulmonary function was poor in many patients with stage I NSCLC who received STI. The minimum %VC and $FEV_{1.0}$% values were as low as 45.4% and 28.1%, respectively. We did not see any relationship between pre-existing pulmonary function, $FEV_{1.0}$% and %VC, and the incidence of RP requiring steroids after STI for stage I NSCLC. Our study could not address the exclusion criteria of %VC, $FEV_{1.0}$%, and DLco from the viewpoint of the risk of RP requiring steroids or oxygen. In other wards, patients with stage I NSCLC are very likely to be good candidates for STI even with poor pulmonary function unfit for the standard treatment, lobectomy. In fact, patients with stage I NSCLC were often inoperable because of poor pulmonary function, and these patients were often referred to STI. Also, not a small proportion of the patients develop secondary NSCLC, not metastasis, after their previous surgery for stage I NSCLC. These patients have poor pulmonary function because of the previous lobectomy, and this study suggests that these are also good candidates for STI.

CONCLUSION

In conclusion, pre-treatment pulmonary function test (%VC, $FEV_{1.0}$%), and dose volume statistics (V_{20}, total dose, BED, dose per fraction, peripheral dose) were not predictive of RP requiring steroid intake after STI for stage I NSCLC. It is still not certain what is the predictor of grade 2 RP in STI from our study. We believe that there must be dose-volume parameters which predict the incidence of RP. Based on the present study, we have started pre-treatment examination of the pulmonary function tests and centralized quality-control study for dose volume statistics including mean lung dose in multi-institutional studies for STI of stage I non-small cell lung cancer. Careful prospective study is mandatory for STI to become a standard treatment for stage I NSCLC.

REFERENCES

1. Lagerwaard FJ, Senan S, van Meerbeeck JP et al. Has 3-D conformal radiotherapy (3D CRT) improved the local tumour control for stage I non-small cell lung cancer? Radiother Oncol 2002;63:151–157.
2. Mehta M, Scrimger R, Mackie R et al. A new approach to dose escalation in non-small-cell lung cancer. Int J Radiat Oncol Biol Phys 2001;49:23–33.
3. Uematsu M, Shioda A, Suda A et al. Computed tomography-guided frameless stereotactic radiotherapy for stage I non-small cell lung cancer: a 5-year experience. Int J Radiat Oncol Biol Phys 2001;51:666–670.
4. Nagata Y, Negoro Y, Aoki T et al. Clinical outcomes of 3D conformal hypofractionated single high-dose radiotherapy for one or two lung tumors using a stereotactic body frame. Int J Radiat Oncol Biol Phys 2002;52:1041–1046.
5. Onimaru R, Shirato H, Shimizu S et al. Tolerance of organs at risk in small-volume, hypofractionated, image-guided radiotherapy for primary and metastatic lung cancers. Int J Radiat Oncol Biol Phys 2003;56:126–135.
6. Timmerman R, Papiez L, McGarry R et al. Extracranial stereotactic radioablation: results of a phase I study in medically inoperable stage I non-small cell lung cancer. Chest 2003;124: 1946–1955.
7. Wulf J, Haedinger U, Oppitz U et al. Stereotactic radiotherapy for primary lung cancer and pulmonary metastases: A noninvasive treatment approach in medically inoperable patients. Int J Radiat Oncol Biol Phys 2004;60:186–196.
8. Onishi H, Araki T, Shirato H et al. Stereotactic hypofractionated high-dose irradiation for stage I nonsmall cell lung carcinoma: clinical outcomes in 245 subjects in a Japanese multiinstitutional study. Cancer 2004;101:1623–1631.
9. Graham MV, Purdy JA, Emami B et al. Clinical dose-volume histogram analysis for pneumonitis after 3D treatment for non-small cell lung cancer (NSCLC). Int J Radiat Oncol Biol Phys 1999;45:323–329.
10. Seppenwoolde Y, Lebesque JV, de Jaeger K et al. Comparing different NTCP models that predict the incidence of radiation pneumonitis. Normal tissue complication probability. Int J Radiat Oncol Biol Phys 2003;55:724–735.
11. Yaes RJ, Patel P, Maruyama Y. On using the linear-quadratic model in daily clinical practice. Int J Radiat Oncol Biol Phys 1991;20:1353–1362.
12. Claude L, Perol D, Ginestet C et al. A prospective study on radiation pneumonitis following conformal radiation therapy in non-small-cell lung cancer: clinical and dosimetric factors analysis. Radiother Oncol 2004;71:175–181.
13. Tsujino K, Hirota S, Endo M et al. Predictive value of dose-vol-

ume histogram parameters for predicting radiation pneumonitis after concurrent chemoradiation for lung cancer. Int J Radiat Oncol Biol Phys 2003;55:110–115.
14. Lee HK, Vaporciyan AA, Cox JD et al. Postoperative pulmonary complications after preoperative chemoradiation for esophageal carcinoma: correlation with pulmonary dose-volume histogram parameters. Int J Radiat Oncol Biol Phys 2003; 57:1317–1322.
15. Kwa SLK, Lebesque JV, Theuws JCM et al. Radiation pneumonitis as a function of mean lung dose: an analysis of pooled data of 540 PTs. Int J Radiat Oncol Biol Phys 1998;28:575–581.
16. Rancati T, Ceresoli GL, Gagliardi G et al. Factors predicting radiation pneumonitis in lung cancer patients: a retrospective study. Radiother Oncol 2003;67:275–283.
17. Robnett TJ, Machtay M, Vines EF et al. Factor predicting severe radiation pneumonitis in PTs receiving definitive chemoradiation for lung cancer. Int J Radiat Oncol Biol Phys 2000;48: 89–94.
18. Inoue A, Kunitoh AH, Sekine I et al. Radiation pneumonitis in lung cancer patients: a retrospective study of risk factors and the long-term prognosis. Int J Radiat Oncol Biol Phys 2001;49:649–655.
19. Gopal R, Starkschall G, Tucker SL et al. Effects of radiotherapy and chemotherapy on lung function in patients with non-small-cell lung cancer. Int J Radiat Oncol Biol Phys 2003;56: 114–120.
20. Hernando ML, Marks LB, Bentel GC et al. Radiation-induced pulmonary toxicity: a dose-volume histograms analysis in 201 patients with lung cancer. Int J Radiat Oncol Biol Phys 2001;51:650–659.
21. Marks LB, Munley MT, Bentel GC et al. Physical and biological predictors of changes in whole-lung function following thoracic irradiation. Int J Radiat Oncol Biol Phys 1997;39:563–570.
22. Lind PA, Marks LB, Hollis D et al. Receiver operating characteristic curves to assess predictors of radiation-induced symptomatic lung injury. Int J Radiat Oncol Biol Phys 2002;54:340–347.

TECHNICAL NOTE

Radiation Medicine: Vol. 23 No. 3, 216–219 p.p., 2005

Simple Technique to Visualize Random Set-up Displacements Using a Commercially Available Radiotherapy Planning System

Hiromichi Ishiyama,* Masashi Kitano,* Yuzuru Niibe,* Mineko Uemae, and Kazushige Hayakawa***

Purpose: To visualize random set-up displacements in isodose distribution images, we introduce a simple technique using a commercially available radiotherapy planning system (RTP).
Materials and Methods: A distribution of set-up displacement is known to be compatible with that of a Gaussian distribution. Based on that assumption, 41 intentionally misaligned beams with 1-mm intervals were planned in the respective weights according to Gaussian distribution. "Modified" isodose distributions were then visualized using a commercially available RTP. In the next step, only two beams misaligned with one standard deviation (SD) of the Gaussian distribution were used in place of 41 beams, as a large number of beams increases the workload and is unsuitable for clinical use. Differences between the two versions of isodose distribution images were assessed visually.
Results: In modified dose distribution images, the edge of distribution was dull compared to normal images. These images show that the larger SD of set-up displacement dulls the edge of dose distribution. Images from two beams were not significantly different to those from 41 beams.
Conclusion: Using this technique, the impact of random set-up displacements was effectively reflected in isodose distribution images.

Key words: set-up displacement, radiotherapy, treatment simulation

Introduction

Geometrical uncertainties in radiotherapy cause differences between intended and actual delivered dose distributions. One of the major causes of uncertainties is set-up displacement.

Set-up displacement can involve systematic and/or random displacement.[1] Systematic displacement comprises the same displacement for each fraction of treatment, whereas random displacement varies from day to day. By measuring set-up displacement several times, the typical sizes of systematic and random displacement can be determined,[2] and the standard deviation (SD) of set-up displacement is reportedly 1.0-5.0 mm for currently applied treatment techniques.[3] In addition, distributions of set-up displacements for all three directions are compatible with that of a Gaussian distribution because of a large number of set-up procedures,[4] and the average and SD of Gaussian distributions are compatible with systematic and random set-up displacement, respectively.

Usually, the margin to expand clinical target volume (CTV) to obtain sufficient tumor coverage is planned empirically by physicians. However, empirical methods could represent a cause of decreased tumor control and increased complications involving normal tissues. In particular, with the recent advent of computed tomography (CT) simulations, isodose distribution images are crucial because of heavy dependence on them by physicians and physicists. For more precise and reasonable planning, we believe that visualization of set-up displacement in isodose distribution images is needed.

This report introduces and assesses a simple technique for visualizing random set-up displacements using a commercially available radiotherapy planning system (RTP).

Received July 16, 2004; revision accepted October 8, 2004.

*Department of Radiology, Kitasato University School of Medicine

**Division of Radiation Oncology, Kitasato University Hospital

Reprint requests to Hiromichi Ishiyama, M.D., Department of Radiology, Kitasato University Hospital, 1-15-1 Kitasato, Sagamihara, Kanagawa 228-8555, JAPAN.

Materials and Methods

Phantom study

A solid water phantom (Solid Water®, Gammex RMI, Middleton, WI, USA) was scanned with a CT simulator using a slice thickness and interval of 5 mm. All images were transferred to a three-dimensional treatment planning system (Pinnacle³®, version 6.5b, ADAC Co., USA). Anterior 10 cm×10 cm irradiations with 4 MV photons were planned. Isodose curves of 110%, 107%, 100%, 95%, 90%, 80%, 70%, 60%, 50%, 40%, 30%, 20%, and 10% relative to an isocenter dose were displayed as a "normal" isodose distribution.

On the assumption that translations of set-up displacements would occur between –20 mm and +20 mm, 41 intentionally misaligned beams were planned with 1-mm intervals along the horizontal axis. Considering the isodose distribution of a total treatment course all at once, the number of fractions at each misaligned beam could be considered the weight of those respective beams. To calculate the weight of each misaligned beam, values of density function of the Gaussian distribution were used. The operational window of Excel software (Microsoft, USA) was used for value calculations (Fig. 1). The average of Gaussian distributions was set on 0 mm, and SDs were set on 1-5 mm, with 1-mm intervals. The five Gaussian distributions were therefore calculated for different SDs and were visualized as "modified" isodose distributions.

Modified isodose distribution images were visually compared with normal isodose distribution images.

Simplification for clinical use

Although a greater number of intentionally misaligned beams makes the Gaussian distribution smoother and more accurate, the workload of operators would be significantly increased. We therefore needed to decrease the number of misaligned beams for clinical use. In principle, as few as two symmetric beams misaligned within 1 SD can be used as a substitute for the large number of misaligned beams, because SD is statistically defined in the literature as a "standard" of deviations. Modified isodose distribution images from two beams were visually compared with those from 41 beams.

Results

"Normal" and "modified" isodose distributions were calculated from 41 beams or two beams (Fig. 2). In modified images, the edge of the distribution was dull

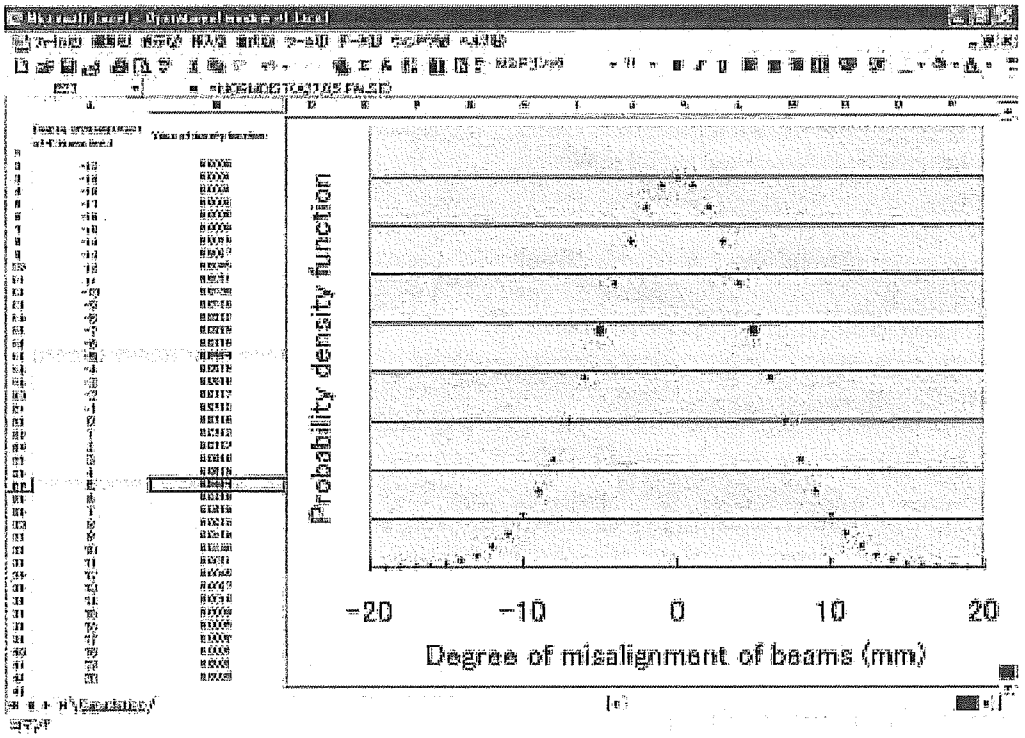

Fig. 1. Values of density function of the Gaussian distribution were calculated using the "NORMDIST" function of Excel software (Microsoft). For calculating the modified isodose distributions from two beams, a pair of symmetric beams misaligned with 1 SD was used (large points in the distribution).

compared to normal images. These images show that a larger SD of set-up displacement dulls the edge of dose distribution. Isodose distribution based on 2 beams was not significantly different from that based on 41 beams.

Clinical case

A case involving prostatic cancer is shown in Fig. 3. The prostate and rectum were manually contoured and planned using a 4-field box technique with 10-MV photons. On the assumption that random set-up displacement within 5-mm SD occurred along all three axes, the isodose distribution image and dose-volume histogram were calculated. Although differences were relatively slight, the impact of random set-up displacement was reflected in both the isodose distribution image and dose-volume histogram.

Discussion

Detailed calculations based on dose coverage of the CTV have been given in a previous report.[5] According to this report, if the SD of systematic errors (Σ) and of random errors (ρ) are known for a specific patient group, the margin M to expand the CTV to a safe planning target volume (PTV) may be expressed as $M = 2\Sigma + 0.7\rho$. With this calculated margin, CTV would be covered with a 95% isodose curve. However, to adapt this calculation to clinical use, manual input of tumor contours is essential. Due to the huge volume of CT data, manual input of all tumor contours for all cases is impractical.

The technique introduced in this report is useful for visually comprehending random set-up displacements, and allows the use of commercially available RTP. Using this technique, it is sufficient to take account of only systematic displacement that is constant during therapy and predictable, rather than random. Systematic displacement of an individual patient can be estimated during the first few fractions, and couch corrections can be applied for subsequent irradiations, although random displacements remain unchanged.[1,6-8] More precise and reasonable planning may be achievable using this technique.

Although this study showed that the isodose distribution based on two beams was not significantly different from that based on 41 beams in a homogeneous phantom study, different distributions may be shown in clinical use with electron density correction. There is need to take account of this point, and further examination is recommended.

Whatever is done to minimize geometrical uncertainties, inaccuracies are to some extent unavoidable. Once typical values for a specific group of patients are known, these should be included in treatment planning for individual patients from that group. Patient set-up displacement not only affects dose in the tumor region, but in neighboring, possibly critical, organs as well. However, the typical size of set-up displacement differs in each institution, as methods of patient fixation and set-up verification systems vary. In addition, beam profiles of linear accelerators differ in each institution. Simulations of data for typical set-up displacement therefore need to be performed at each institution. For this reason, availability of a simple, standard technique is crucial, and our technique can be applied to any institution. Using the technique introduced in this paper, the impact of random set-up displacements can be effectively reflected in isodose distribution images.

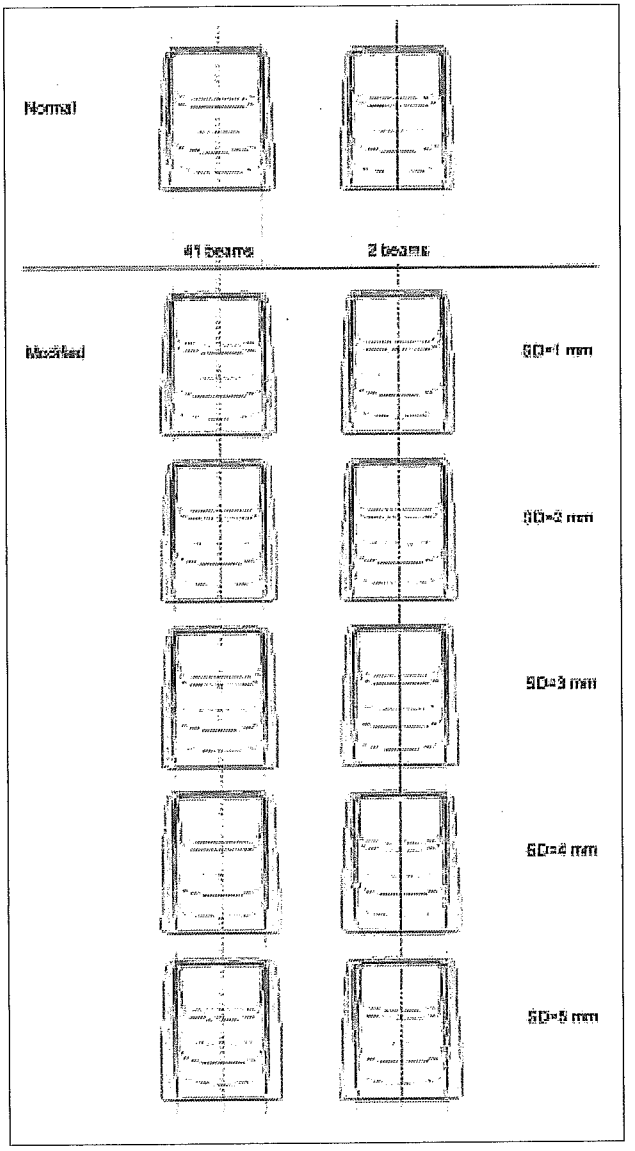

Fig. 2. Modified isodose distributions were calculated from two beams or 41 beams. The portal size was 10 cm×10 cm.

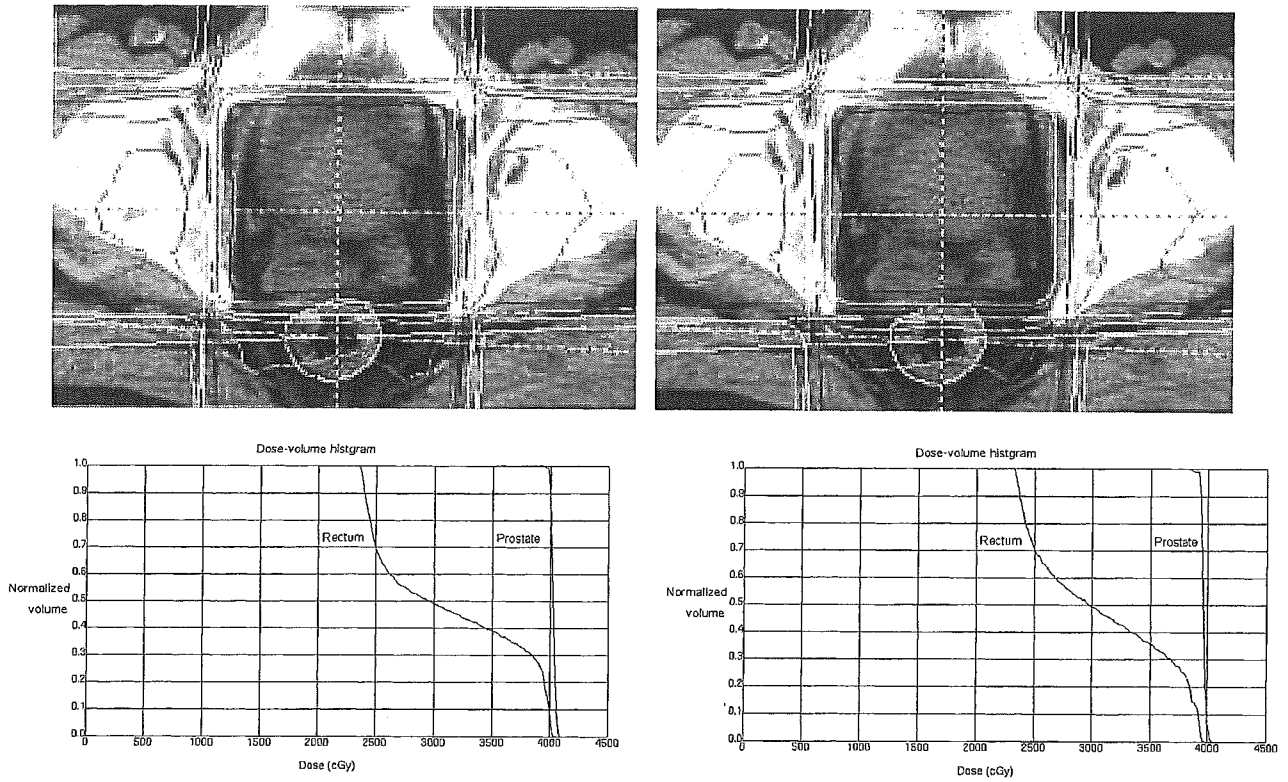

Fig. 3. Edge of the isodose distribution was sharp in normal distribution (A) and dull in modified distribution (B). Dose-volume histograms of the prostate and rectum reflect differences between normal (C) and modified (D) distributions.

A	B
C	D

ACKNOWLEDGEMENTS

This work was supported in part by Grant-in-Aid for Scientific Research from Japan Society for the Promotion of Science and the Ministry of Health, Labour and Welfare in Japan.

REFERENCES

1) Bel A, van Herk H, Bartelink H, Lebesque JV. A verification procedure to improve patient set-up accuracy using portal images. *Radiother Oncol*, 29: 253–260, 1993.
2) Bijhold J, Lebesque JV, Hart AA, Vijlbrief RE. Maximizing setup accuracy using portal images as applied to a conformal boost technique for prostatic cancer. *Radiother Oncol*, 24: 261–271, 1992.
3) Hurkmans CW, Remeijer P, Lebesque JV, Mijnheer BJ. Set-up verification using portal imaging; review of current clinical practice. *Radiother Oncol*, 58: 105–120, 2001.
4) Rudat V, Flentje M, Oetzel D, Menke M, Schlegel W, Wannenmacher M. Influence of the positioning error on 3D conformal dose distributions during fractionated radiotherapy. *Radiother Oncol*, 33: 56–63, 1994.
5) Stroom JC, de Boer HC, Huizenga H, Visser AG. Inclusion of geometrical uncertainties in radiotherapy treatment planning by means of coverage probability. *Int J Radiat Oncol Biol Phys*, 43: 905–919, 1999.
6) Yan DD, Wong JW, Gustafson G, Martinez A. A new model for "accept or reject" strategies in off-line and on-line megavoltage treatment evaluation. *Int J Radiat Oncol Biol Phys*, 31: 943–952, 1995.
7) Yan D, Wong J, Vicini F, *et al.* Adaptive modification of treatment planning to minimize the deleterious effects of treatment setup errors. *Int J Radiat Oncol Biol Phys*, 38: 197–206, 1997.
8) Boer HCJ, Heijmen BJM. A protocol for the reduction of systematic patient setup errors with minimal portal imaging workload. *Int J Radiat Oncol Biol Phys*, 50: 1350–1365, 2001.

Role of Mitochondrial DNA in Cells Exposed to Irradiation: Generation of Reactive Oxygen Species (ROS) is Required for G2 Checkpoint upon Irradiation

Saori Kawamura,[a] Daisaku Takai,[a] Keiko Watanabe,[a] Jun-ichi Hayashi,[b] Kazushige Hayakawa,[c] and Makoto Akashi*,[a]

[a]Department of Radiation Emergency Medicine, Research Center for Radiation Emergency Medicine, National Institute of Radiological Sciences, 4–9–1 Anagawa, Inage-ku, Chiba 263–8555, Japan, [b]Institute of Biological Sciences, University of Tsukuba, 1–1–1 Tennodai, Tsukuba, Ibaraki 305–8572, Japan, and [c]Department of Radiology, Kitasato University School of Medicine, 1–15–1 Kitasato, Sagamihara, Kanagawa 228–8555, Japan

(Received February 4, 2005; Accepted February 7, 2005)

Mitochondria have their own genome encoding subunits of the electron transport chain. Using cells lacking mitochondrial DNA (mtDNA, ρ^0 cells), we studied the role of mtDNA in irradiation. Loss of mtDNA inhibited cell growth and reduced the level of reactive oxygen species (ROS) as compared to ρ^+ cells. ρ^+ cells were more resistant to irradiation than ρ^0 cells. Upon irradiation, ρ^0 cells showed delayed G2 arrest and decreased ability of a cell to recover from the G2 checkpoint compared to ρ^+ cells. Irradiation increased the generation of ROS even more in ρ^+ cells. Irradiation markedly increased the levels of phosphorylated forms of extracellular-regulated kinases, p42 and p44 (ERK1/2) in ρ^+ cells, whereas phosphorylated levels of the kinases were affected slightly in ρ^0 cells. Furthermore, inhibition of the ERK pathway led to a delayed G2 arrest and a delayed recovery from the arrest in irradiated ρ^+ cells, and treatment with NAC also induced dysfunction of the G2 checkpoint in irradiated ρ^+ cells. These results suggest that the accumulation of ROS potentiated ERK1/2 kinases after irradiation in ρ^+ cells, leading to less sensitivity to irradiation. Thus, mtDNA is important for the generation of ROS that act as second messenger.

Key words —— mitochondrial DNA, irradiation, reactive oxygen species, checkpoint

INTRODUCTION

Mitochondria have their own DNA (mtDNA) of 16 kilo base pairs in human cells. mtDNA encodes subunits of the mitochondrial electron transport chain. These subunits are essential for normal oxidative phosporylation and also adenosine triphosphate (ATP) production in a cell. Oxidative phosphorylation in mitochondria produces the large part of the energy required within a cell.[1)] Human mtDNA has a mutational rate at least 10 times higher than nuclear DNA,[2)] and somatic mutations in mtDNA have also been observed in human neoplasms.[3)] Recently, there have been reports using cells lacking mtDNA that studied its roles in cell death or sensitivity to various external insults. Studies have shown that mtDNA-depleted cells are susceptible to cell death by serum-deprivation, tumor necrosis factor (TNF) and staurosporine.[4–6)] On the other hand, studies found that these cells were more resistant to insults such as tumor necrosis factor-related apoptosis-inducing ligand (TRAIL), anti-cancer reagents, and reactive oxygen species (ROS) than their parental cells.[7,8)] Thus, the roles of mtDNA are still not clear, and the mechanisms for the sensitivity to external insults remain unresolved.

The respiratory chain in mitochondria is a source of ROS.[9–12)] On the other hand, studies have shown that ROS generated in mitochondria can modulate signaling cascades.[13–15)] The pathway of the mitogen-activated protein kinase (MAPK) family is involved in growth factor-mediated regulation of diverse cellular events such as proliferation, senescence, differentiation and apoptosis.[16)] Exposure of cells to oxidative stress such as irradiation induces activation of multiple MAPK pathways; these signals play critical roles in controlling cell survival and repopulation effects following irradiation.[16)] The MAPK superfamily is composed of several signal-

*To whom correspondence should be addressed: Department of Radiation Emergency Medicine, Research Center for Radiation Emergency Medicine, National Institute of Radiological Sciences, 4–9–1 Anagawa, Inage-ku, Chiba 263–8555 Japan. Tel.: +81-43-206-3122; Fax: +81-43-284-1736; E-mail: akashi@nirs.go.jp

ing pathways: mitogen-activated extracellular-regulated kinases, p42 and p44 (ERK1/2), c-Jun N-terminal kinase (JNK), and p38 pathways. ERK1/2 are serine/threonine kinases that are regulated by mitogen-activated/extracellular-regulated kinase 1/2 (MEK1/2) through phosphorylation. The activation of ERK1/2 protects cells against noxious stimuli in several ways and inhibits apoptosis through the activation of caspase or the inhibition of cytochrome c release.[17,18] Furthermore, ERK1/2 activation has been reported to promote several transcriptional factors such as nuclear factor-kappa B (NF-κB) and cyclic adenosine monophosphate responsive element binding protein (CREB), which then stimulate the expression of anti-apoptotic genes.[19] The activation of ERK1/2 has been reported to abrogate the G2/M phase arrest after irradiation in some cell types.[20,21] In contrast, JNK and p38 MAPK have been reported to mediate caspase activation, resulting in apoptosis.[16] However, the roles of mtDNA and how ROS generated in mitochondria affect signaling pathways are not fully understood in cells exposed to irradiation.

The recent progress in studies of mitochondria has allowed us to use mtDNA-depleted cells (ρ^0cells) and their control cells (ρ^+ cells). Elimination of mtDNA from cells can be performed by long-term exposure to a low concentration of 3,8-diamino-5-ethyl-6-phenylphenanthridinium bromide (ethidium bromide; EtBr).[22] ρ^+ cells are produced by the fusion of cytoplasts from the parent cells with ρ^0 cells, and these cells possess normal mtDNA. By comparing ρ^0 to ρ^+ cells, the roles of mtDNA can be determined. Irradiation is well known to induce apoptosis and cause DNA damage. However, there are few studies on the roles of mtDNA in irradiated cells. In the present study, we investigated the roles of mtDNA in irradiated cells by comparing ρ^0 cells lacking mtDNA and their control ρ^+ cells. We found that ρ^0 cells were more radiosensitive than ρ^+ cells, and demonstrated that homeostatic mitochondrial ROS production may have a protective effect on cells exposed to irradiation through MEK activation and cell cycle control.

MATERIAL AND METHODS

Cells and Cell Culture —— Cells used in this study originated from HeLa cells: ρ^0 cells (EB8-C) lacking mtDNA, and ρ^+ cells (HeEB5) cybrid clones produced by fusion of EB8-C cells and cytoplasts of HeLa cells.[22,23] For cell culture, the medium consisted of RPMI 1640 (Gibco, Invitrogen Corp., CA, U.S.A.) supplemented with 10% (v/v) fetal bovine serum (INTERGEN, Purchase, NY, U.S.A.), 50 μg/ml of uridine (Sigma, St. Louis, MO, U.S.A.) and 1 mM of sodium pyruvate (Gibco).

Polymerase Chain Reaction (PCR) —— Total DNA was extracted by the phenol/chloroform method. Primers were specific for the segment of mitochondrial DNA: forward, 5′-atg ccc caa cta aat act acc g-3′ and reverse, 5′-gtg gtg att agt cgg ttg ttg a-3′. After electrophoresis on 2% agarose, the 298-bp fragment was analyzed with ethidium bromide (Sigma) under UV light.

Clonogenic Assays —— For colony formation assay, 10^2 to 5×10^3 cells were seeded in 60-mm culture plates 18 hr before irradiation at various doses. Colonies were stained and counted after 14 days; groups of cells containing at least 50 cells were defined as a colony. Colonies with diameter greater than 1.2 mm were defined as "larger colonies" using Intelligent Quantifier™ (Bio Image Systems, Inc., Jackson, MI, U.S.A.). Survival curves are representative data from three independent experiments.

Radiation Setting —— ^{137}Cs source emitting at a fixed dose rate of 10 Gy/min was used for γ-ray irradiation.

Cell Cycle Analysis —— After irradiation, cells were fixed with 70% ethanol at the times indicated. Then the cells were incubated for 30 min at 37°C with 1 μg/ml RNase A, stained with 50 μg/ml propidium iodide and filtered through nylon mesh with a pore size of 50–70 μm. Cell cycle profiles were evaluated by FACScaliber flow cytometry (Becton Dickinson, Bedford, MA, U.S.A.).

Analysis of Intracellular ROS Production —— 2′,7′-dichlorofluorescein (DCF) is one of the most prevalent oxidant-sensitive fluorescent dye. Acetyl ester derivative of dihydro-DCF diacetate (CM-H_2DCFDA, Molecular Probes, Eugene, OR, U.S.A.), a derivative of DCF, was used in this study. Cells were prepared 18 hr before the treatment to a cell count of 6×10^5 for each 60-mm diameter dish. After irradiation, cells were stained with 10 μM CM-H_2DCFDA at 37°C for 5 min. Fluorescence intensity was measured by flow cytometry with excitation at 488 nm and emission at 530 nm.

Western-Blot Analysis —— The cells were lysed in buffer containing 50 mM Tris–HCl (pH 8.0), 150 mM NaCl, 3 mM NaN_3, 0.1% (w/v) sodium dodecyl sulfate (SDS), 1% (v/v) Nonidet P-40 and 0.5% sodium deoxycholate. The protein concentra-